Article

In-Rich Surface Growth on P-Rich InP(001) (2 × 1) Surface: Structural and Mechanistic Study

Indrajit Bandyopadhyay, and Krishnan Raghavachari

J. Phys. Chem. C, **2008**, 112 (15), 6022-6026 • DOI: 10.1021/jp709682c

In-Rich Surface Growth on P-Rich InP(001) (2 × 1) Surface: Structural and Mechanistic Study

Indrajit Bandyopadhyay and Krishnan Raghavachari*

Department of Chemistry, Indiana University, Bloomington, Indiana 47405

Received: October 3, 2007; In Final Form: January 4, 2008

Metal−organic chemical vapor deposition (MOCVD) is a widely used method for the growth of compound semiconductor surfaces using gas-phase precursors. In this work, we have used density functional calculations and cluster models to investigate the growth of the In-rich indium phosphide surface resulting from the chemical reaction of InH_3 with the P-rich (2 × 1) surface. In particular, the thermodynamics and kinetics of the individual steps involved in the growth are considered thoroughly. The highest barrier corresponds to the initial reaction involving InH_3 dissociation on the phosphorus dimer. The detailed mechanisms as well as the energetics of the different steps are discussed.

Introduction

The polar InP(001) surface is technologically very important, widely used in optoelectronic devices, high-power electronics, and as a substrate for epitaxial wafer growth.[1−3] The surface preparation is commonly carried out using metal−organic chemical vapor deposition (MOCVD) using gas-phase III/V precursors such as phosphine/tertiarybutyl phosphine and trimethyl indium. Under typical MOCVD conditions, the layer-by-layer growth of InP film on InP(001) wafer is normally carried out at a high substrate temperature of ∼600 °C. An understanding of the growth process that governs the epitaxial film quality is clearly of fundamental importance.

Although the surface chemistry of indium phosphide is complex, some of the surface phases have been well characterized. For example, the most common P-rich surface phase, InP-(001) (2 × 1), is known to have a hydrogen-stabilized structure consisting of buckled phosphorus dimers.[4−7] The most common In-rich phase has a complex (2 × 4) reconstruction involving the presence of adatom dimers. The P-rich and In-rich surfaces can be stabilized by annealing at about 300 and 650 °C, respectively, in a UHV chamber, and have been characterized using spectroscopic techniques and surface stress measurements.[8−10] Although some reactivity studies on P-rich and In-rich surfaces have been done both experimentally and theoretically to improve InP-based devices,[11−18] the detailed mechanism of InP film growth from the decomposition of III−V precursors is not well understood. Our objective is to understand the kinetics and thermodynamics of heterogeneous gas-phase reactions of the precursor molecules with the P-rich and In-rich surfaces leading to epitaxial growth.

In this paper, a mechanistic pathway of the growth of the In-rich surface over P-rich InP(001)-(2 × 1) is presented. The pathway comprises of several steps that have been considered individually. We use InH_3 as the simplest precursor molecule and have not attempted to investigate the role of defects on the growth chemistry. The whole study has been done using computationally tractable, reasonably sized cluster models. For some of the key steps with the largest barriers, larger cluster models have been used to ensure convergence of results. To the best of our knowledge, there have been no similar studies of the In-rich surface growth mechanisms. In a future study, we plan to report the growth of a P-rich surface starting from an In-rich surface. It will be interesting to perform a similar study for other compound semiconductors such as GaAs to see how the constituent atoms influence the growth chemistry and to understand the mechanistic aspects that are common to different compound semiconductors.

Theoretical Methods

A 4 × 1-sized cluster model ($In_{13}P_{15}H_{34}$) with two P dimers was used as the starting point in our work. An important point to note here is the nature of the truncated bond terminations used in our cluster models. Although typical cluster models use hydrogen atoms to terminate all of the truncated bulk bonds, such a scheme is not appropriate for III−V semiconductors because of the presence of dative bonding contributions between the elements. To achieve a proper balance between covalent and dative bonding in our cluster model, two of the second-layer indium atoms are terminated with phosphine molecules, while the remainder of the bulk In and P atoms are truncated with hydrogens. We have shown previously that such a scheme yields an appropriate local tetra-coordination of the elements while maintaining a proper balance between covalent and dative bonding.[18]

Geometries were optimized initially with the density functional theory (DFT) method using the standard B3LYP functional[19,20] (Becke's three parameter exchange functional combined with the gradient-corrected correlation functional of Lee, Yang, and Parr) in conjunction with the "sdd" basis set[21,22] [Stuttgart−Dresden relativistic pseudopotential (Pd-core) along with the associated double-ζ basis set for In; Dunning/Huzinga double-ζ basis set (D95) for P and H]. All structures were optimized with the atomic coordinates constrained from the third layer and below along tetrahedral directions with In−P = 2.54 Å; In−H = 1.76 Å; P−H = 1.42 Å. A careful vibrational analysis at the B3LYP/sdd level was performed to confirm the nature of the stationary points and to get zero-point energy corrections. The application of structural constraints in the cluster surface model introduces artificial forces that must be accounted for properly in the cluster frequency calculations. In

* Corresponding author. E-mail: kraghava@indiana.edu.

10.1021/jp709682c CCC: $40.75
Published on Web 03/26/2008

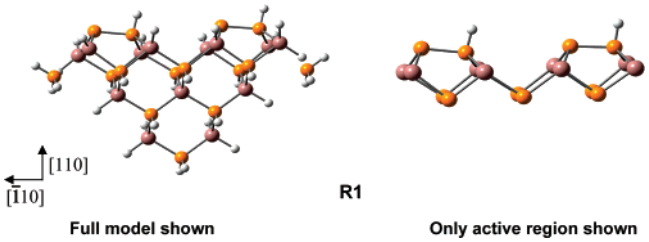

Figure 1. Structure of the 4 × 1-sized cluster model ($In_{13}P_{15}H_{34}$) used in the calculations (P, yellow; In, brown).

this work, to eliminate the erroneous forces during the frequency calculations, infinite masses were assigned to the fixed atoms in building the mass-weighted Hessian. All minima were confirmed to have all positive frequencies while transition states have one imaginary frequency yielding the appropriate reaction coordinate. In order to get more reliable geometries and relative energies, additional geometry optimizations were done using an all-electron (18s/14p/9d)/[6s/5p/3d] contracted basis set for In atoms and a polarized double-ζ D95** basis set for P and H atoms.[23] These calculations will be denoted as "B3LYP/large" in the rest of the paper. The transition state involved in the final step was not optimized at this level because of convergence problems.

Although the cluster model as defined above is appropriate for investigating In insertion into P dimers (leading to P−In−P linkages), it is too small to study In−In dimer formation. Hence, a suitable larger 4 × 2-sized cluster model ($In_{24}P_{24}H_{44}$), which is the doubled unit cell of the intermediate after second InH_3 adsorption and subsequent H_2 desorption (vide infra), was considered for studying the In−In dimer bond formation.

All of the calculations were carried out using the Gaussian03 suite of programs.[24]

Results and Discussion

Under the typical conditions used in MOCVD, it is known that the P-rich (2 × 1) surface has a hydrogen-stabilized structure. In particular, it consists of a complete layer of buckled phosphorus dimers with every other P atom terminated with hydrogen. Thus, we start from a structure consisting of H−P−P: dimer units where ":" denotes the presence of a lone pair on the "up" atom of the buckled dimer. The vapor-phase precursor molecule used in our study is InH_3, and we explore a sequence of chemical reactions starting from such a P-rich surface leading to the growth of an In-rich surface layer.

The complete mechanism consists of four elementary steps. They are the following: step I, nonactivated physisorption of InH_3 followed by dissociative chemisorption; step II, Intradimer P−In−P bridge formation through H_2 desorption; step III, InH_3 adsorption and interdimer P−In−P bridge formation through H_2 desorption; step IV. In−In dimer bond formation. The structure of the full model that was used in this study including all saturating atoms/groups is shown at the top left of Figure 1, and a simplified two-layer representation focusing on the active sites is shown at the top right of Figure 1. In order to maintain the flow of the discussion, we will show only the simplified structures in each of the individual steps.

TABLE 1: Relative Energies and Enthalpies (kcal/mol) of all of the Species Involved in Steps I−IV[a]

	step I				step II		
	R1 + InH_3	**RC1**	**TS1**	**P1**	**P1**	**TS2**	**P2**
ΔE_e	0.0	−16.2	14.0	−29.9	0.0	19.0	−11.8
ΔE_0	0.0	−15.1	14.4	−27.7	0.0	18.0	−14.0
ΔH_{298}	0.0	−14.9	14.1	−27.4	0.0	17.3	−13.0
$\Delta H'_{298}$					−27.4	−10.1	−40.4

	step III				step IV		
	P3′	**P3**	**TS3**	**P4**	**R2**	**TS4**	**P5**
ΔE_e	0.0	−4.5	28.9	1.1	0.0	(32.4)	0.9
ΔE_0	0.0	−5.0	27.3	−2.5	0.0	(30.5)	−0.8
ΔH_{298}	0.0	−4.7	27.2	−2.1	0.0	(30.3)	0.7

[a] ΔE_e and ΔE_0 are the B3LYP/large relative energies without and with zero-point correction (calculated from unscaled B3LYP/sdd harmonic frequencies), respectively. ΔH_{298} are the corresponding relative enthalpies at 298 K. The enthalpies ($\Delta H'_{298}$) of the species in step II are relative to the starting materials, viz. **R1** and InH_3. The relative energies of **TS4** have only been computed at the B3LYP/sdd level and are listed in parenthesis.

We now discuss the key points of each reaction step.

Step I. Nonactivated InH_3 Physisorption and Dissociative Chemisorption. The structures of the species involved in the individual steps are shown in Figure 2, and the corresponding potential energy curves are shown in Figure 3. Indane (InH_3) physisorbs onto a P-dimer site via dative bonding between the lone pair of the "up" P atom of the dimer and the vacant orbital

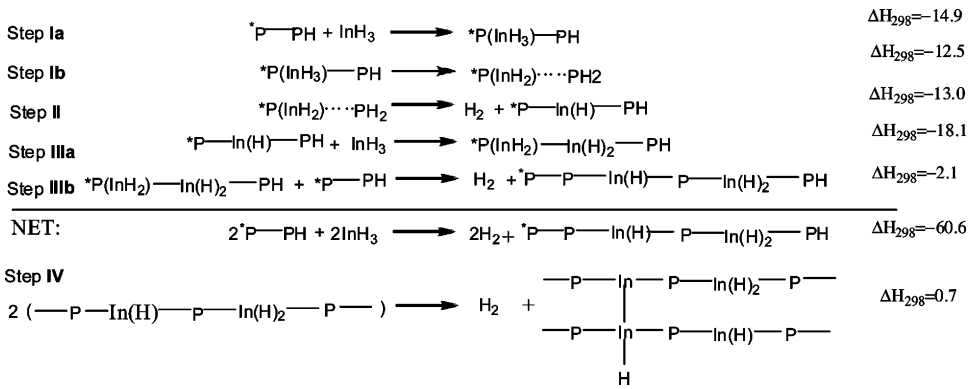

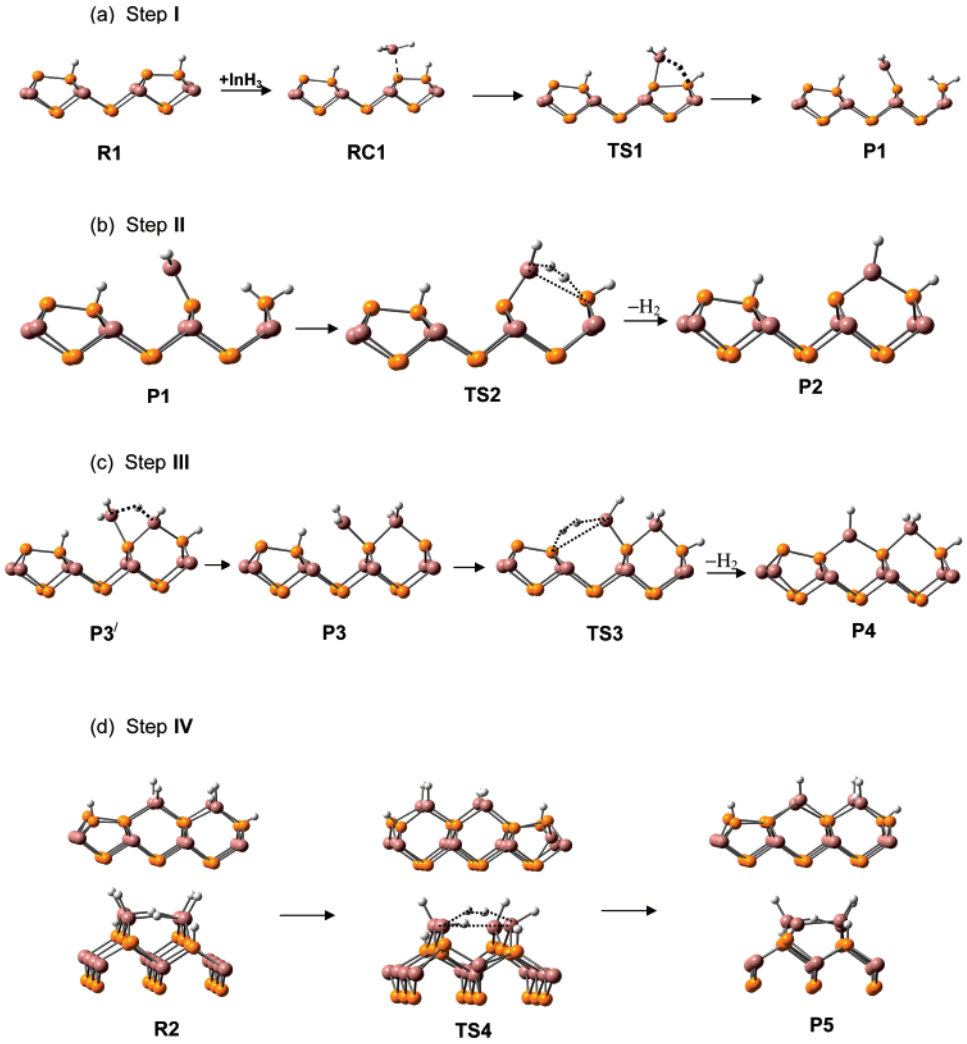

Figure 2. The four elementary steps of the complete mechanism of In-rich surface growth on P-rich InP(001) (2 × 1) surface. (a) Step I, nonactivated InH_3 physisorption and subsequent dissociative chemisorption. (b) Step II, intradimer P−In−P bridge formation via H_2 desorption. (c) Step III, interdimer P−In−P bridge formation via H_2 desorption. (d) Step IV, In−In dimer bond formation through H_2 desorption from reacting InH_x species.

of In. The resulting Lewis adduct (**RC1**) has a stabilization energy of 15 kcal/mol and an In···P bond distance of 2.80 Å. As expected, the dative bonded distance is about 0.30 Å larger than a typical In−P covalent distance, 2.50 Å in **P1** (vide infra). Moreover, the complex is a metastable minimum and can form a more stable structure (**P1**) via a hydrogen migration to the other P of the dimer, leading to the breaking of the dimer bond. The corresponding energy barrier is significant, ∼14 kcal/mol with respect to the bare cluster and InH_3, with the four-centered transition structure, **TS1**, leading to the formation of the dissociated chemisorbed product, **P1**. In the transition structure, the partially formed P···H (1.73 Å) and partially broken P···P (2.61 Å) bonds are easily identified, while the migrating hydrogen from InH_3 shows an elongated In···H distance (1.99 Å). The adsorption exothermicity of **P1** with respect to the bare cluster and InH_3 is 30 kcal/mol, and the corresponding desorption barrier is 44 kcal/mol. The transition structure was confirmed by the presence of one imaginary frequency (729i cm^{-1}). The normal coordinate motion corresponding to the imaginary frequency shows that it follows the expected reaction coordinate. The P−InH_2 covalent bond length in **P1** is 2.50 Å. The calculated energy barrier for desorption from **P1** is much greater than that of dissociation (see step II). Our results can be compared with the results of PH_3 dissociative chemisorption on an In−P mixed dimer as well as on an In−In dimer of the In-rich InP(001) $\delta(2 \times 4)$ surface reported by Das et al.[25] In the former case, the barrier is about 12 kcal/mol, whereas in the latter case it is about 20 kcal/mol. But the associative desorption barrier was considerably less for PH_3 chemisorbed on the In−P dimer (30 kcal/mol) than that of InH_3 on the P-rich surface in the present study, whereas for PH_3 chemisorbed on In−In(43 kcal/mol) the values are somewhat similar.

This elementary reaction is the highest barrier step in the overall mechanism. Zero-point and thermal corrections (298 K) were calculated using a rigid rotor harmonic oscillator model, and the stabilization enthalpy of **RC1** is 15 kcal/mol. The corresponding forward barrier is 14 kcal/mol, the exothermicity is 27 kcal/mol, and the reverse barrier is 42 kcal/mol. To check the reliability of our calculations for this crucial step, we performed calculations on a small 2 × 1-sized cluster model ($In_5P_6H_{17}$) as well as a very large 4 × 2-sized cluster model ($In_{20}P_{24}H_{40}$) and the results were within 4 kcal/mol.

Vibrational spectroscopy is an indispensible tool for successful identification and characterization of the species involved in various steps. Typically, computed harmonic frequencies are too high compared to experiment, and we have previously used empirical correction factors of about 100 cm^{-1} to take into account systematic overestimation of the computed frequencies. For the species involved, the stretching frequencies (uncorrected) of the chemisorbed InH_2 fragment in **P1** are 1784 and 1791 cm^{-1} and the two surface P−H stretching frequencies appear at 2315 and 2380 cm^{-1} (the respective bond lengths are 1.421

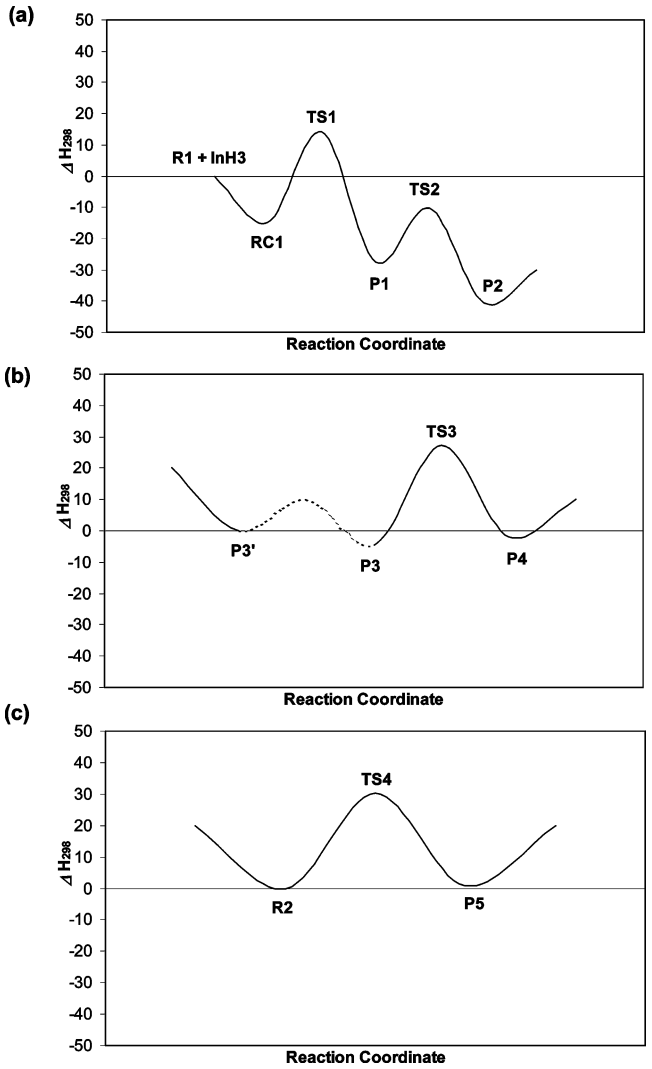

Figure 3. Reaction profiles of the steps (a, steps I and II; b, step III; c, step IV) of the complete mechanism of In-rich surface growth on P-rich InP(001) (2×1) surface at the B3LYP/large level except **TS4** where B3LYP/sdd values have been employed (see text for details). All relative enthalpies are in kcal/mol.

and 1.415 Å). The physisorbed InH_3 frequencies in **RC1** occur at 1692, 1716, and 1740 cm^{-1} and are red-shifted with respect to bare InH_3, as expected. The substrate−adsorbate stretching vibration in **P1** occurs at 365 cm^{-1}.

Step II. Intradimer P−In−P Bridge Formation via H_2 Desorption. The InH_2 and PH_2 species react on the surface to form an intradimer P−In−P bridge with the desorption of H_2. Because of the large distance between the dimers, interdimer P−In−P bridge formation at this step is unlikely. The product (**P2**) is stabilized relative to **R1** and InH_3 by about 42 kcal/mol. This step is exothermic by 12 kcal/mol. and the associated energy barrier with respect to **P1** is 19 kcal/mol. In **TS2**, the distance between the two desorbing hydrogens is 1.00 Å, whereas the In···H and P···H distances are 1.96 and 1.80 Å, respectively. Thus, the bonds with the desorbing hydrogens (P−H and In−H) are elongated by 0.38 and 0.20 Å, respectively. The normal coordinate motion corresponding to the imaginary frequency at the transition state **TS2** shows that it follows the expected reaction coordinate. In the bridged InH species (**P2**), the InH stretching frequency occurs at 1795 cm^{-1}. The two substrate−adsorbate stretchings occur at low frequencies, 331 and 291 cm^{-1}. The two surface PH stretches appear at 2305 and 2353 cm^{-1}. Although the zero-point corrected barrier for this exothermic step is ∼18 kcal/mol, the corresponding transition state **TS2** occurs substantially below the transition state **TS1** for the first step (Figure 3a). Overall, at the zero-point corrected level, P−In−P bridge-bond formation over the phosphorus dimer (here called the intradimer In bridge) is characterized by an energy barrier of 18 kcal/mol, an enthalpy barrier of 17 kcal/mol, an exothermicity at 298 K of 13 kcal/mol, and a reverse barrier of about 30 kcal/mol.

Step III. Interdimer P−In−P Bridge Formation via H_2 Desorption. The growth of an In-rich layer also requires In insertion between two adjacent dimers. To investigate this, we optimized a structure (**P3′**) obtained after a second InH_3 adduct formation at the P site aligned toward the interdimer region (Figure 2c). Because of the presence of a neighboring trivalent In site formed in the previous step and the propensity of indium to form bridging In−H−In linkages, the adduct **P3′** contains a hydrogen migrating to the bridging position between two In atoms. However, **P3′** is easily transformed into a slightly exothermic (∼4 kcal/mol at B3LYP/large) tetrahydride substrate phase (**P3**), which further undergoes dehydrogenation to form an interdimer bridged form (**P4**) as shown in Figure 2c. The hydrogen desorption (ΔE_0) is about 3 kcal/mol exothermic. The desorption barrier, corresponding to the associated transition state **TS3**, is about 30 kcal/mol. As in other cases, the transition structure (**TS3**) was confirmed by the presence of one imaginary frequency and the nature of its associated reaction coordinate. At the zero-point corrected level, the energy barrier, enthalpy barrier, and exothermicity at 298 K relative to **P3** are 27, 27, and 2 kcal/mol, respectively.

It is of interest to compare the interdimer In insertion seen in this step with the intradimer insertion seen in the previous step. It is clear from our work that the interdimer insertion (step III) is energetically more expensive, kinetically as well as thermodynamically, compared to intradimer In insertion (step II) with an enthalpy barrier larger by ∼10 kcal/mol and less exothermic by ∼11 kcal/mol. This is clearly a consequence of the larger distance of the interdimer P atoms that makes it more difficult to insert an indium in the intervening space.

The intermediate (**P3′**) is characterized by the H of InH_3 disposed between two In atoms with In···H distances of 2.069 and 1.904 Å. It is also important to investigate the characteristic frequencies of the moieties P−In(H)−P and P−In$(H)_2$−P formed in this step. In the product **P4**, the frequencies of bridged InH_2 and InH moieties occur at 1776, 1768, and at 1794 cm^{-1}, respectively. For comparison, in **P3′** the symmetric and antisymmetric stretching frequencies associated with the InH_2 moiety resulting from partially dissociated InH_3 appear at 1814 and 1834 cm^{-1}.

Step IV. In−In Dimer Bond Formation through H_2 Desorption from Reacting InH_x Species. The previous steps considered above lead to the formation of −P−In(H)−P−In$(H)_2$−P− groups on the surface. As mentioned earlier, we have used a larger cluster model with coupling between two such groups to investigate In dimer formation on the surface. The species involved in this step are shown in Figure 2d. The In−In dimer formation in this step is characterized by a barrier height of 32 kcal/mol at the B3LYP/sdd level. The process is slightly endothermic. However, this reaction occurs with the requirement of no additional external energy in the reaction conditions because the reaction is energetically well below the starting materials.

The reactant (**R2**) has rows of alternating InH_2 and InH surface species along $<\bar{1}10>$ as the P−In(H)−P−In$(H)_2$−P moiety. The neighboring units are staggered with respect to each

other so that the InH_2 of one unit is aligned with the InH of the neighboring unit. The InH_2 groups tilt toward the neighboring InH unit to form partially bridged bonds. This can be clearly seen in the In−H distances in InH_2 groups of 1.73, 1.86, 1.73, and 1.89 Å at the B3LYP/sdd level. The two longer bonds are due to the formation of the In···H bridge bonds whose distances correspond to 1.96 and 1.92 Å. The four stretching frequencies for the bonds of terminal hydrogens with In are at 1792, 1813, 1819, and 1824 cm^{-1}. As expected, the two frequencies associated with two In···H···In bridge bonds are red-shifted significantly. **R2** forms an In−In dimer bonded structure (**P5**) via the four-centered transition structure (**TS4**). The transition structure (**TS4**) is characterized rigorously as in other cases by its imaginary frequency and the associated normal coordinate motion. The distance between two desorbing hydrogens is 1.091 Å in the transition state. The product **P5** has an H−In−In unit with an In−In distance of 2.98 Å (2.95 Å at B3LYP/large) and an In−H distance of 1.73 Å (1.75 Å at B3LYP/large). At the final zero-point corrected thermochemical level at 298 K, the enthalpy barrier relative to **R2** is 30 kcal/mol at the B3LYP/sdd level. At the B3LYP/large level, the exothermicity (ΔE_0) is about 1.0 kcal/mol.

Overall, we have started from an appropriate cluster model representing a hydrogen-stabilized P-rich InP(001) (2 × 1) surface. A sequence of reactions involving the addition of two molecules of InH_3 followed by three H_2 elimination reactions leads to the formation of an In−In dimer unit, the simplest unit needed to form an In-rich surface. Although additional reactions need to be considered in the future, our paper provides the basic groundwork to understand a key growth step leading from a P-rich surface to an In-rich surface.

Concluding Remarks

The mechanism of In-rich surface growth over the P-rich 2 × 1 InP(001) surface has been studied here at the B3LYP level of theory with two different basis sets. The structures, vibrational frequencies, and relative stabilities of the species involved have been computed. The kinetics and thermodynamics of each step have also been investigated. The slowest step is the InH_3 dissociation over the phosphorus dimer with a barrier of ∼14 kcal/mol. Our results appear to be converged with respect to cluster size ($In_5P_6H_{17}$ and $In_{20}P_{24}H_{40}$). The B3LYP/sdd results are consistent with the larger basis set (B3LYP/large). Interdimer P−In−P bridge formation in the intervening space between two phosphorus dimers along the $<\bar{1}10>$ direction is energetically more expensive, kinetically as well as thermodynamically, compared to intradimer P−In−P bridge formation (step II) with a barrier larger by ∼10 kcal/mol and less exothermic by ∼11 kcal/mol. In conclusion, this study clearly sets the framework for the growth of In/V compound semiconductors, and it will be interesting to see if similar aspects govern the growth of other compound semiconductors such as GaAs.

Acknowledgment. We gratefully acknowledge funding from the Petroleum Research Fund (PRF 43465-AC10) and from NSF (CHE-0616737).

References and Notes

(1) INSPEC (Information service) *Properties of Indium Phosphide*; INSPEC: London, 1991.
(2) Swaminathan, V.; Macrander, A. T. *Material Aspects of GaAs and InP Based Structures*; Prentice Hall: Englewood Cliffs, NJ, 1991.
(3) *Properties, Processing and Applications of Indium Phosphide*; Pearsall, T. P., Ed.; INSPEC: London, 1999; p 271.
(4) Seong, H.; Lewis, L. J. *Surf. Sci.* **1995**, *337*, 166.
(5) Jin, J.-M.; Lewis, L. J. *Surf. Sci.* **1995**, *325*, 251.
(6) Fu, Q.; Negro, E.; Chen, G.; Law, D. C.; Li, C. H.; Hicks, R. F.; Raghavachari, K. *Phys. Rev. B* **2002**, *65*, 075318.
(7) Schmidt, W. G.; Hahn, P. H.; Bechstedt, F.; Esser, N.; Vogt, P.; Wange, A.; Richter, W. *Phys. Rev. Lett.* **2003**, *90*, 126101.
(8) Law, D. C.; Fu, Q.; Visbeck, S. B.; Sun, Y.; Li, C. H.; Hicks, R. F. *Surf. Sci.* **2002**, *496*, 121.
(9) Fuster, D.; Gonzalez, M. U.; Gonzalez, Y.; Gonzalez, L. *Surf. Sci.* **2006**, *600*, 23.
(10) Li, L.; Fu, Q.; Li, C. H.; Han, B. K.; Hicks, R. F. *Phys. Rev. B* **2000**, *61*, 10223.
(11) Woo, R. L.; Das, U.; Cheng, S. F.; Chen, G.; Raghavachari, K.; Hicks, R. F. *Surf. Sci.* **2006**, *600*, 4888.
(12) Sun, Y.; Law, D. C.; Visbeck, S. B.; Hicks, R. F. *Surf. Sci.* **2002**, *513*, 256.
(13) Sun, Y.; Law, D. C.; Hicks, R. F. *Surf. Sci.* **2003**, *540*, 12.
(14) Morral, A. F. I.; Zahler, J. M.; Griggs, M. J.; Atwater, H. A.; Chabal, Y. J. *Phys. Rev. B* **2005**, *72*, 085219.
(15) Wang, C. X.; Pitts, O. J.; Watkins, S. P. *J. Cryst. Growth* **2003**, *248*, 259.
(16) Kumar, S.; Michael, G. S.; Lisa, B. L.; Weinberg, W. H.; Yates, J. T., Jr.; Kenneth, C. J. *J. Chem. Phys.* **1990**, *92*, 5700.
(17) Pluchery, O.; Chabal, Y. J.; Opila, R. L. *J. Appl. Phys.* **2003**, *94*, 2707.
(18) Raghavachari, K.; Fu, Q.; Chen, G.; Li, L.; Li, C. H.; Law, D. C.; Hicks, R. F. *J. Am. Chem. Soc.* **2002**, *124*, 15119.
(19) Lee, C.; Yang, W.; Parr, R. G. *Phys. Rev. B* **1988**, *37*, 785.
(20) Becke, A. D. *J. Chem. Phys.* **1993**, *98*, 5648.
(21) Igel-mann, G.; Stoll, H.; Preuss, H. *Mol. Phys.* **1988**, *65*, 1321.
(22) Dolg, M.; Wedig, U.; Stoll, H.; Preuss, H. *J. Chem. Phys.* **1987**, *86*, 866.
(23) Godbout, N.; Salahub, D. R.; Andzelm, J.; Wimmer, E. *Can. J. Chem.* **1992**, *70*, 560.
(24) Frisch, M. J.; Trucks, G. W.; Schlegel, H. B.; Scuseria, G. E.; Robb, M. A.; Cheeseman, J. R.; Montgomery, J. A., Jr.; Vreven, T.; Kudin, K. N.; Burant, J. C.; Millam, J. M.; Iyengar, S. S.; Tomasi, J.; Barone, V.; Mennucci, B.; Cossi, M.; Scalmani, G.; Rega, N.; Petersson, G. A.; Nakatsuji, H.; Hada, M.; Ehara, M.; Toyota, K.; Fukuda, R.; Hasegawa, J.; Ishida, M.; Nakajima, T.; Honda, Y.; Kitao, O.; Nakai, H.; Klene, M.; Li, X.; Knox, J. E.; Hratchian, H. P.; Cross, J. B.; Bakken, V.; Adamo, C.; Jaramillo, J.; Gomperts, R.; Stratmann, R. E.; Yazyev, O.; Austin, A. J.; Cammi, R.; Pomelli, C.; Ochterski, J. W.; Ayala, P. Y.; Morokuma, K.; Voth, G. A.; Salvador, P.; Dannenberg, J. J.; Zakrzewski, V. G.; Dapprich, S.; Daniels, A. D.; Strain, M. C.; Farkas, O.; Malick, D. K.; Rabuck, A. D.; Raghavachari, K.; Foresman, J. B.; Ortiz, J. V.; Cui, Q.; Baboul, A. G.; Clifford, S.; Cioslowski, J.; Stefanov, B. B.; Liu, G.; Liashenko, A.; Piskorz, P.; Komaromi, I.; Martin, R. L.; Fox, D. J.; Keith, T.; Al-Laham, M. A.; Peng, C. Y.; Nanayakkara, A.; Challacombe, M.; Gill, P. M. W.; Johnson, B.; Chen, W.; Wong, M. W.; Gonzalez, C.; Pople, J. A. *Gaussian 03*, revision C.02; Gaussian, Inc.: Wallingford, CT, 2004.
(25) Das, U.; Raghavachari, K.; Woo, R. L.; Hicks, R. F. *Langmuir* **2007**, *23*, 10109.